Participating Institutions

The following 12 Japanese institutions participated in this multi-center study: Azabu Neurosurgical Hospital, Sapporo City; Asahikawa Red Cross Hospital, Asahikawa City; Handa City Hospital, Handa City; Ichinomiya Municipal Hospital, Ichinomiya City; Kashiwaba Neurosurgical Hospital, Sapporo City; Japanese Red Cross Kobe Hospital, Kobe City; Nakamura Memorial Hospital, Sapporo City; National Cardiovascular Center, Osaka; Ogori Daiichi General Hospital; Yamaguchi City; Oji General Hospital, Tomakomai City; Sunagawa City Medical Center, Sunagawa City; Teine Keijinkai Hospital, Sapporo City.

Introduction

Single Photon Emission Computed Tomography (SPECT) is widely available in clinical institutions, but current clinical practice relies largely on interpretation of qualitative images reflecting physiological function. It has been demonstrated that quantitative functional parametric images may be obtained by applying mathematical modeling to SPECT data corrected for attenuation and scatter. Quantitative regional cerebral blood flow (rCBF) (*1-3*) and cerebral vascular reactivity in response to acetazolamide challenge (CVR) (*4-6*) have been able to be obtained with these techniques. One major application of such quantitative SPECT approaches is the evaluation of ischemic status in patients with occlusion/stenosis in their middle cerebral arteries, with particularly emphasis on providing prognostic information of the likely outcome of revascularization therapies (*7*). In addition, quantitative analysis in SPECT has also been demonstrated in the assessment of binding potential for several neuro-receptor ligands (*8,9*). More recently, quantitative SPECT was further promoted for quantitative assessment of regional myocardial perfusion (*10,11*), and also for assessing radioaerosol deposition and clearance in healthy and diseased lungs (*12*). While the quantitative potential of SPECT is well recognized, providing the standardized approach required for multi-center clinical trials has so far received only limited attention. Challenges remain in providing consistent quantitative data across institutions using a variety of different SPECT imaging equipment and vendor specific reconstruction strategies (*13*). This limitation is largely due to a lack of standardized procedures in the reconstruction software offered by vendors, particularly in terms of correcting attenuation and scatter. The necessary kinetic modeling for physiological parameter estimation is also not provided by the SPECT vendors as part of the standard software offered. While separate packages can be purchased for this purpose, they are not integrated and are flexible general purpose packages, which require considerable skill and knowledge to effectively use them, thus they are not ideal for routine clinical use.

Recent studies have demonstrated that appropriate compensation for both attenuation and scatter can provide reconstructed images with reasonable accuracy. Scatter and attenuation occur in the object and are thus object dependent, but are not dependent on the geometry of imaging equipment (*14*). Therefore, once a software program is developed to provide accurate image reconstruction with compensation for both attenuation and scatter, the program should be able to provide quantitative images that are intrinsically independent of the geometric design of SPECT cameras. This is an attractive feature of SPECT for multi-center clinical studies.

From the various techniques available to correct for attenuation (*15*) and scatter (*16*), one approach, which has been considered feasible for application in clinical studies, is based on a combination of attenuation correction incorporated into the ordered-subset maximum-likelihood expectation maximization (OSEM) reconstruction (*17*), and scatter correction by the transmission-dependent convolution subtraction (TDCS) originally proposed by Meikle et al (*18*). Adequacy of this approach has been extensively investigated in our group (*11,19*), for ^{99m}Tc both for brain and heart (*18,20*), and also in cardiac ^{201}Tl studies (*11,21*). A recent study also demonstrated the accuracy of this approach in a combined CT/SPECT system

(*22*). Application has been further extended to the ^{123}I isotope, by incorporating a correction for collimator septal penetration by the high-energy emission from ^{123}I and the low level impurities in commercially supplied ^{123}I (*11*).

The quantitative SPECT reconstruction approach has been applied in a clinical setting to estimate CBF images at rest (*11*), and also to quantitate cerebral vascular reactivity by measuring CBF at rest and after vasodilation in a single SPECT imaging session. This was accomplished by using the Dual-Table Autoradiographic (DTARG) method and a dual administration of ^{123}I-iodoamphetamine (^{123}I-IMP) (*23*). In those studies, both corrections for attenuation and scatter appeared to be essential for generating quantitative CBF maps that were consistent with those by ^{15}O-water PET (*11,23*). Quantitative reconstruction is also of importance when applying the compartment-model based kinetic approach to extract two independent CBF images from a single session dual injection and dual SPECT scan protocol.

However, these studies were validated in a single institution using a limited range of SPECT systems and the general applicability of this technique for different SPECT systems had yet to be fully established. Thus the aim of this study was to verify that analysis of data with a standardized reconstruction package incorporating attenuation and scatter can provide reproducible results across institutions for quantitative rest and acetazolamide challenge CBF estimation from a single SPECT scanning session (*23*) in a multicenter study.

Materials and Methods

Institutions and subjects

The 12 participating institutions were clinical centers and generally did not have scientific staff dedicated to nuclear medicine software/hardware development. Standard, vendor supplied software was used for the collection of the studies, using unmodified scanners and collimators clinically used for brain studies. The acquired data were reconstructed with the program package developed for this project. Manufacturers and models of camera systems, the number of detectors, collimators (including fanbeam or parallel hole), utilized in the institution are listed in Table 1. All institutions carried out experiments on physical phantoms according to the protocol described below. Of the twelve institutions, nine institutions carried out patient scans, while the remaining three institutions provided only phantom data. Clinical studies were approved by institutions' ethics committees or followed guidelines for clinical research protocols authorized in the institution. All subjects gave written informed consent in each institution.

The clinical studies were divided into 3 protocols, (a) the intra-institutional, intra-subject reproducibility (Reproducibility), (b) comparison with PET (VS PET), and (c) the intra-scan consistency of the dual time-point split dose protocol (Rest-Rest). Studies were excluded from the analysis if there was severe patient motion during one of the studies or if there were changes in the condition of the patients between the 1st and 2nd study likely to lead to changes in CBF.

Eight institutions (#1, #3, #4, #6, #8, #9, #11 #12) participated to the "Reproducibility" arm, in which quantitative CBF values measured on separate days were compared (at least 3 pairs of scans at each institution). In this arm, all patients suffered from unilateral or bilateral stenosis or occlusion in the extracranial internal carotid artery. The ages ranged from 43 to 81 year old (mean ± sd; 65 ± 9). There were a total of 31 studies in this protocol which were analyzed. A further 4 patients had to be excluded from analysis as follows: Two patients were reported to have significant changes in their patho-physiological status between the studies, and additional two patients showed severe movement in one of the two scans, as well as improper positioning of one of the two patients in the field-of-view of the SPECT camera.

One institution (#4) performed the "VS-PET" studies. CBF values obtained by the DTARG method were compared with

those by O-15 water and PET. Studies were carried out on 6 patients (5 male, 1 female) with stenosis or occlusion of extra-cranial internal carotid artery unilaterally (n = 3) or bilaterally (n = 3). Their ages ranged from 71 to 74 year old (mean ± sd; 72 ± 1).

Two institutions (#2 and #12) provided data for "Rest-Rest" comparison. Consistency of the two CBF values estimated from the scans after the 1st and 2nd injection in the double administration protocol was evaluated. There was no pharmacological challenge in these patients, thus the CBF estimates from the two scans should be the same. Five patients from institution #2 had chronic cerebral infarction, while four subjects from institution #13 had no sign of cerebral disease. Their age ranged from 32 to 72 (mean ± SD; 52 ± 15), and 5 male, 4 female.

Phantom experiment

Three sets of experiments were carried out in each institution using the SPECT camera fitted with the collimators normally used in clinical brain studies. The first scan was designed to determine the absolute sensitivity or the Becquerel calibration factor (BCF) of the reconstructed images for each acquisition system. A syringe filled with ^{123}I-IMP solution of known radioactivity was placed at the center of FOV and a complete 360 deg projection set was acquired for 10 min. The syringe was supplied by a radiopharmaceutical company (Nihon Medi Physics, Tokyo,Japan) and its radioactivity was calibrated to be 111MBq at noon on the day before the experiment with an accuracy better than 3%. At the time of the experiment the activity had decayed to approximately 30 MBq in each institution. This lower activity avoided significant losses due to dead time and better reflected activity in the brain during clinical studies. The BCF factor was determined by dividing the absolute radioactivity by the total counts for the syringe region in the reconstructed image.

The second experiment was carried out to determine the septal penetration contribution (*24*) from high energy photons into the primary 159 keV energy window for ^{123}I for each collimator. A single line source was filled with ^{123}I-IMP, and a line-spread function (LSF) was obtained from the projection data. The background level was determined from these projection data as the penetration contribution from high-energy photons as described previously (*19*). This line source was also placed in a cylindrical phantom of 16 cm diameter filled with water, and LSF was also generated from the projection data for this phantom. The septal penetration compensation as well as the scatter correction were confirmed with the projection data from this experiment.

The third experiment used a uniform cylindrical phantom of 16 cm in diameter, and 15 cm in length, filled with ^{123}I-solution. The whole radioactivity used for the BCF determination was diluted into the phantom, and projection data were acquired for 30 min, according to the same protocol as for the clinical scans described below. Approximately 0.3 mL of solution in the phantom was sampled after the SPECT scanning, and its radioactivity concentration (counting rate per unit mass) was measured using the well counters available in the various institutions. Both NaI and plastic scintillator based well counters were used (Table 1). An ROI was placed to measure the average pixel counts of the reconstructed emission images, and the value was referred to the radioactivity count rate assessed by the well counter, to determine the cross-calibration factor (CCF) between the SPECT images and the well counter system, which was subsequently used to count the blood samples from the clinical studies. Uniformity of the reconstructed emission images for this phantom was evaluated both in-plane and also in the axial direction.

Clinical studies

All clinical SPECT studies essentially followed the DTARG protocol with dual administration of IMP (*25*). The procedure is diagrammatically depicted in Figure 1. Briefly, two dynamic scan were carried out in quick succession, with a 2 min interval between the scans. The first scan essentially covered the initial 0-28 min period, and second was acquired from 30 to 58 min. The time per

frame was 4 min, requiring 7 frames to cover each of the 2 dynamic scan periods. ^{123}I- IMP (111 MBq – Institutions 2-12 or 167 MBq at Institution #1) was infused twice over 1 min into the antecubital vein at the time of each SPECT scan initiation, namely at 0 min and at 30 min. Acetazolamide (16 mg/kg, 1,000 mg maximum) was administered intravenously at 20 min after the first IMP injection, which corresponds to 10 min before the 2nd IMP injection. Projection data were summed for the whole acquisition duration of the 1st and 2nd scans, and reconstructed according to the reconstruction procedures described below. In contrast with the previous article of Kim et al (*25*) which used full arterial blood sampling, the individual arterial input functions were derived from a population-based standardized input function. The population based input function was scaled based on the whole blood counts from a single arterial blood sample taken at approximately 10 min (*1,26,34,36,37*). This sample was also used for arterial blood gas analysis.

In the "reproducibility" arm, an additional CBF study was carried out, beside the DTARG protocol, on a separate day. The protocol was based on the previously reported IMPARG method (*1,19,26*), and was performed within a month of the DTARG study. The IMPARG method is essentially equivalent to the present DTARG method, except that the IMPARG method uses a single IMP administration to assess CBF either at rest or after acetazolamide challenge. The same image reconstruction process as for the DTARG protocol was employed. In 12 studies, DTARG protocol was employed instead of IMPARG, namely the DTARG study was performed twice to assess the CBF reproducibility at rest and after acetazolamide.

In the VS PET protocol, the PET study was carried out within 2 days of the DTARG-SPECT study. PET scans used intravenous ^{15}O-water both at rest and after the acetazolamide challenge. CBF images were calculated by the ^{15}O-water autoradiography technique as previously reported (*27*), with careful corrections for delay and dispersion (*28-30*). Patients were stable between the SPECT and PET with no further episodes of ischemic disease or neurological deficits.

In the Rest-Rest protocol, the DTARG scan was carried out without the pharmacological challenge during the scan, and the consistency of the two CBF values estimated from the first and second scans were evaluated.

Quantitative SPECT reconstruction (QSPECT)

A program package was developed using a platform and wrapper written in JAVA to run several programs written in C for Microsoft Windows systems. The package includes programs for reconstructing SPECT images from projection data, calculating functional images, performing image co-registration and reslicing, and printing summary logs.

Images were reconstructed from the original projection data obtained from the commercial SPECT equipment, based on previous works of Iida and his colleagues (*19-21,23,31,32*) at each institution. The reconstruction program provides SPECT counts in units of Bq/mL, which are independent of scanning parameters such as the acquisition time, the number of views, matrix size, zoom factor, etc. Standard uniformity and centre of rotation corrections and fan-beam to parallel beam conversion (for fan beam collimators) were performed using the vendors' standard software prior to reconstruction by this package. In one institution (Institute #4), a generalized program for the fan-beam to parallel beam conversion supplied by a third-party vendor was utilized.

An overall flow diagram of the correction and reconstruction process is shown in Figure 2. The OSEM reconstruction technique was employed, which includes attenuation correction (*17*). A threshold based edge detection algorithm was applied to generate the attenuation mu map, assuming a uniform attenuation co-efficient of 0.166 cm^{-1} for ^{123}I as an average over the brain and the

skull (*19*). The threshold was optimized via the user interface to provide correct definition of the brain outline. The attenuation μ-map was generated from the rest frame obtained for the 0-28 min period, and was co-registered to the other images (*35*) obtained by the conventional filtered-back projection (FBP) technique without attenuation or scatter correction. The attenuation μ-map were forward projected to provide the attenuation projection data required for TDCS. Scatter was subtracted from the emission projections based on the TDCS method, as originally proposed by Meikle et al (*18*), and further optimized for realistic ^{99m}Tc, ^{201}Tl, and ^{123}I data in the brain and thorax regions (*20,21,23,31,32*). An offset in the TDCS process compensated for the septal penetration of high energy photons for ^{123}I studies which adds fairly uniform background counts or "DC" component to the projections.

Scatter and attenuation corrected images where reconstructed with OSEM (5 iterations, 5 subsets using geometric-mean projections, post reconstruction Gaussian filter with 7 mm full-width at half maximum) and then aligned again to the image set obtained from the first scan. Pixel counts in the reconstructed images were normalized by the acquisition duration, pixel size, the number of views, the number of detectors and the BCF to convert the pixel counts to units of Bq/mL.

Functional CBF images at rest and after acetazolamide challenge were calculated based on a single-compartment model from single session dynamic SPECT acquisitions, essentially by the method of Kim et al. (*23*). Significant clearance of IMP from the brain is taken into account by implementing a parameter of distribution volume, and residual IMP concentration in the brain is also implemented in the kinetic analysis to estimate both rest and elevated CBF's from a single session of dynamic SPECT acquisition. Since only a single arterial blood sample was taken to calibrate the previously determined population-based arterial input function, the short-period SPECT images taken for 24-28 min was employed to calculate the global CBF over the entire grey matter, as this timing minimizes the individual variation of the shape in individual input function on the CBF estimation. The look-up table generated for estimating CBF images from the complete dynamic study (0-28 min) was then scaled to provide CBF values consistent with those from the 24-28 min frame in the entire cortical grey matter region. A careful detection algorithm was employed to reliably exclude extra-cranial accumulation of ^{123}I-IMP such as in the parotid region which could adversely affect this scaling procedure. The regional CBF was then estimated at each pixel by means of the Table-Look-Up (TLU) procedure (*26,37*). The background image at the time of second injection of ^{123}I-IMP was estimated from the first phase CBF images according to the compartment model assumed in this study (*25*). An additional TLU procedure was applied to the second dynamic data set (30-58 min) for calculating the vaso-dilated (acetazolamide challenge) CBF images as described previously (*25*).

Data analysis

The activity estimated in the uniform phantom from the SPECT counts were compared to the known activity injected into the phantom. Images for the baseline study were displayed with subsequent images using an absolute flow value scale to visually ascertain regional as well as global differences in flow. Regions-of-interest (ROI) were placed on the middle cerebral artery territories of both hemispheres, and the average flow values between the different methods were compared and plotted. Bland-Altman plots and the standard deviation of the differences evaluated the consistency of CBF values obtained from the Reproducibility, and VS-PET protocols.

All data were presented as mean ± 1 s.d. *Pearson's* correlation analysis and linear regression analysis were used to evaluate relationships between the two CBF values. $p<0.05$ was considered statistically significant.

Results

Phantom Studies

Figure 3 shows data from the line source in the 16 cm scattering cylinder without

and with scatter correction. The uncorrected line source images show the background counts extending beyond the phantom caused by the septal penetration of the high energy photons. The scatter correction is largely effective in correcting for scatter as well as the septal penetration counts. The Toshiba-ECAM LMEGP collimator, which is designed for reduced septal penetration when imaging ^{123}I, shows reduced scatter as well as reduced septal penetration counts compared to standard low energy GE LEHR collimator. The lower septal penetration of the Toshiba-ECAM LMEGP collimators is also supported by a lower scatter correction offset value of DC=0.05 compared to DC=0.20 for the GE LEHR collimator. The reduced scatter and septal penetration results in more complete removal of scatter for the LMEGP collimator.

Figure 4 displays reconstructed slices of the uniform phantom for all 12 institutions, scaled to the same maximum activity concentration. The estimated activity concentrations from these studies compared with the known activity concentration in the phantom are shown in Table 1 (%-Difference Column). Pixel counts of the uniform cylindrical phantom represent the absolute radioactivity concentration, eg, in units of Bq/mL, (with an accuracy of 87.5 +/- 5.1%). The well counter-to-SPECT cross calibration factor, or CCF, which represents the sensitivity of the well counter system for ^{123}I radioisotope was 0.5-1.0 for the system with NaI, and in the order of 0.1-0.2 for the systems with plastic scintillation detectors. It can also be seen from Table 1 that the BCF values were consistent for the same SPECT camera/collimator configurations.

Clinical Studies

Figure 5a shows typical CBF images obtained at 4 institutions with different 4 gamma camera vendors, performed as part of the reproducibility arm of the study. Figure 5b shows CBF images from one subject in one institution for slices covering the whole brain. The images clearly demonstrate that the DTARG method can reliable detect cerebral vascular reactivity in response to acetazolamide both in terms of increase in global flow as well as changes in regional distribution of flow. The image quality of the CBF images after Diamox is not visually different from those at rest, nor from those acquired on the separate day. The acetazolamide images performed by DTARG method are in good agreement with the images subsequently performed with the IMPARG method post acetazolamide infusion. Similarly, images performed at rest with DTARG agree well with the images subsequently performed with IMPARG method at rest (Figure 5a, the last column, rows 1 and 3). The good reproducibility is confirmed by the Bland-Altman plot comparison of DTARG CBF values with the CBF values obtained at a different imaging session with IMPARG or DTARG (Figure 5c). The standard deviation of the differences is 5.2 ml/100g/min, with low bias support by the mean difference of 0.4 ml/100g/min. Regression analysis between DTARG and IMPARG values yielded a significant correlation ($p<0.001$), with a correlation coefficient of $r=0.93$.

Figure 6a shows MRI and CBF images at rest and after acetazolamine obtained with DTARG-SPECT and ^{15}O-water PET on a 74 year old female patient (48 kg) with left internal-carotid artery stenosis. Normal CBF but reduced CBF reactivity in the left MCA territory was visible in both SPECT and PET images. Figure 6b also shows MRI and CBF images in a 73 year old male patient (63 kg) with right internal-carotid artery stenosis and left internal-carotid occlusion. CBF was reduced at rest and did not respond to acetazolamide in both SPECT and PET images. Figure 6c compares the flow values obtained at rest and post acetazolamide with DTARG with the corresponding values obtained by ^{15}O-water PET. The standard deviation of the differences is 5.1 ml/100g/min, with the significant underestimation compared to PET by the DTARG method highlighted by a mean difference of -6.1 ml/100g/min. The Pearson's analysis resulted in significant correlation ($p<0.001$) with a correlation coefficient of $r=0.88$.

The results from the "rest-rest" protocol are summarized in Figure 7. The

differences between the measurements performed with the first injection and with the second injection are small and there is good agreement between the two flow values. The mean and standard deviation of the differences are 0.6 ± 2.9 ml/100g/min.

Discussion

In this study, we demonstrated that the use of the QSPECT package provided quantitative images consistent between the participating centers, using dual or triple detector SPECT scanners and collimators routinely employed for non-quantitative brain studies. All centers could successfully perform the dynamic SPECT acquisitions on their standard SPECT scanners and the data from the variety of cameras encountered were successfully processed by the package. It was also shown that rest CBF and cerebral vascular reactivity can be readily obtained in a single, clinically practical, 1hr scanning session by the participating institutions. Good reproducibility of CBF estimates was observed in 31 pairs of studies in 8 institutions (Figures 5a-5c), and the CBF estimated with the ^{123}I-IMP SPECT agreed well with ^{15}O-water PET CBF in one institution (Figures 6a-6c). The CBF values following the 2nd injection of the DTARG were consistent with the values obtained after the 1st injection when no vasodilating stress was given in 9 studies at 2 institutions (Figure 7).

Quantitative cerebral blood flow and cerebral vascular reactivity in response to acetazolamide challenge can be of significant prognostic value for patients being considered for revascularization of cerebral arteries (*5-7*). The previously validated IMPARG method can provide such information, but requires two independent scans on difference days to assess the two CBFs at rest and post-acetazolamide challenge (*5-7*). This was a crucial limiting factor for routine clinical studies. The recently proposed DTARG protocol to quantitatively assess CBF both at rest and after acetazolamide in a single dynamic SPECT imaging session with dual administration of ^{123}I-IMP (*23*) makes the protocol much easier for clinical patients. It is also apparent that errors caused by ambiguity of the absolute scaling, as well as possible changes in physiological status of the subjects between scans can be reduced substantially with the DTARG protocol. The quantitative reconstruction program enabled the compartment model-based kinetic analysis to compensate for the residual radioactivity concentration during the 2nd session of the dynamic scan.

Major error sources in SPECT, namely the attenuation and scatter, are only object dependent (*14*) and not gamma camera or collimator dependent, and thus SPECT images obtained by this quantitative reconstruction package should be generally consistent across systems. Septal penetration of high energy photons for ^{123}I is, however, collimator dependent (*24*), but could be compensated as part of the TDCS scatter correction algorithm (*11*) as demonstrated in Figure 3. Consistency in estimating the absolute radioactivity concentration was supported by the uniform cylindrical phantom experiment. The radioactivity concentration of the uniform cylinder phantom estimated in units of Bq/mL showed variation within +/- 5.1% (Figure 4 and Table 1), though systematic underestimation by 12.5%. This systematic underestimation is attributed to the BCF factor being derived from a line source in air experiment, reconstructed without scatter, attenuation and septal penetration corrections. However, this underestimation does not affect the CBF estimation, as it relies on the direct cross calibration between the gamma counter used to count the blood sample and the SPECT measurements.

This phantom study also highlighted the importance of proper calibration and Quality Control (QC) of the gamma camera as well as current and appropriate uniformity and centre of rotation corrections to avoid artifacts and bias in the reconstructed images. These corrections are applied, as for other clinical studies, by the vendors' software, rather than as part of the QSPECT system, as these corrections are typically carried out on-line and on-the-fly, with only the corrected data being stored.

The previously validated population based input function requiring only a single arterial blood sample for scaling (*1,26,34,36,37*) has been incorporated in the present package, as the typical multiple and frequent arterial blood sampling is not compatible with routine clinical use. Blood from this single arterial sample is also used to measure arterial blood gases, which are relevant and of interest clinically in these patients. The timing of the single blood sample (approximately 10 min post IMP injection) was optimized previously (*1,26,34,36,37*) to minimize the errors associated with individual differences in shape of the arterial input function compared to the population average curve. In addition, absolute global CBF was estimated from SPECT images taken at an optimized mid-scan time of approximately 30 min (or 24-28 min), rather than from the initial part of the study, in order to minimize the population based input function scaling errors (*1,26,34,36,37*). Thus, to achieve maximum accuracy for scaling, CBF was first calculated using the data from the 24-28 min frame only, and the regional CBF images were calculated from the early SPECT images acquired for 0-28 min in this package, as described in the Materials and Method section.

Partial volume correction has not been implemented as part of this processing protocol. Partial volume effects can potentially lead to underestimation of flow values in grey matter regions due to the limited resolution of SPECT. The small underestimation of 6.1 ml/100g/min by DTARG when compared to ^{15}O-water PET (Figure 6c) is attributed to the partial volume effect due to differences in resolution between PET and SPECT. In addition, it could lead to variations in CBF values obtained with different collimators with different intrinsic resolution. However, consistent post reconstruction filtering, as applied in this study, can reduce this effect, but the effects of different spatial resolution on blood flow estimates warrant further investigation.

Two studies had to be omitted from the analysis due to patient motion, and improper positioning of the patient in the field-of-view of the SPECT camera. For these cases, general purpose rotating gamma cameras rather than the brain-dedicated systems were used. Such problems may be minimized by careful positioning of the patient head in the scanner and using appropriate head fixation devices.

Only the reproducibility within an institution was assessed. Hence the reproducibility of measurements between institutions can not be gleaned from these data, particularly since patient with vascular disease were studied. Thus unlike estimates from normal volunteers, flow values and vascular reactivity are expected to vary from patient to patient, so flow values determined at one institution with one group of patients are not directly comparable with flow values from another group of patients in another institution due to likely real CBF differences between the groups. A realistic brain phantom, such as recently developed by our group could be used to assess the consistency of brain activity concentration measurements between institutions and this study is in the planning phase.

Conclusion

A quantitative package (QSPECT) has been developed which allows absolute cerebral blood flow and cerebral vascular reactivity to be estimated in a routine clinical environment. This multi-center study has demonstrated its applicability in a variety of clinical settings and for a variety of equipment. Results from the "Reproducibility", "VS PET", and "Rest-Rest" studies suggest that a change of approximately 10 % or 5 ml/min/100 g can be readily detected in follow-up clinical studies using this technique. The graphical user interface (GUI) for easily controlling the inbuilt sophisticated programs and tools ensures that routine use does not require dedicated support from scientific or computing staff. The package is now successfully used in over 130 institutions in Japan and more than 25,000 patient studies have been analyzed with the QSPECT package.

References

1. Iida H, Akutsu T, Endo K, et al. A multicenter validation of regional cerebral blood flow quantitation using [^{123}I]iodoamphetamine and single photon emission computed tomography. *J Cereb Blood Flow Metab* 1996; 16: 781-793.
2. Hatazawa J, Iida H, Shimosegawa E, Sato T, Murakami M, Miura Y. Regional cerebral blood flow measurement with iodine-123-IMP autoradiography: normal values, reproducibility and sensitivity to hypoperfusion. *J Nucl Med* 1997; 38: 1102-1108.
3. Yamaguchi T, Kanno I, Uemura K, et al. Reduction in regional cerebral metabolic rate of oxygen during human aging. *Stroke.* 1986; 17: 1220-1228.
4. Ogasawara K, Ito H, Sasoh M, et al. Quantitative measurement of regional cerebrovascular reactivity to acetazolamide using 123I-N-isopropyl-p-iodoamphetamine autoradiography with SPECT: validation study using H2 15O with PET. *J Nucl Med.* 2003; 44: 520-525.
5. Ogasawara K, Ogawa A, Terasaki K, Shimizu H, Tominaga T, Yoshimoto T. Use of cerebrovascular reactivity in patients with symptomatic major cerebral artery occlusion to predict 5-year outcome: comparison of xenon-133 and iodine-123-IMP single-photon emission computed tomography. *J Cereb Blood Flow Metab.* 2002; 22: 1142-1148.
6. Ogasawara K, Ogawa A, Yoshimoto T. Cerebrovascular reactivity to acetazolamide and outcome in patients with symptomatic internal carotid or middle cerebral artery occlusion: a xenon-133 single-photon emission computed tomography study. *Stroke.* 2002; 33: 1857-1862.
7. Ogasawara K, Ogawa A. [JET study (Japanese EC-IC Bypass Trial)]. *Nippon Rinsho.* 2006; 64 Suppl 7: 524-527.
8. Fujita M, Ichise M, Zoghbi SS, et al. Widespread decrease of nicotinic acetylcholine receptors in Parkinson's disease. *Ann Neurol.* 2006; 59: 174-177.
9. Deloar HM, Watabe H, Kudomi N, Kim KM, Aoi T, Iida H. Dependency of energy and spatial distributions of photons on edge of object in brain SPECT. *Ann Nucl Med.* 2003; 17: 99-106.
10. Iida H, Eberl S, Kim KM, et al. Absolute quantitation of myocardial blood flow with (201)Tl and dynamic SPECT in canine: optimisation and validation of kinetic modelling. *Eur J Nucl Med Mol Imaging.* 2008; 35: 896-905.
11. Iida H, Eberl S. Quantitative assessment of regional myocardial blood flow with thallium-201 and SPECT. *J Nucl Cardiol.* 1998; 5: 313-331.
12. Eberl S, Chan HK, Daviskas E, Constable C, Young I. Aerosol deposition and clearance measurement: a novel technique using dynamic SPET. *Eur J Nucl Med.* 2001; 28: 1365-1372.
13. Hapdey S, Soret, M., Ferrer, L., Koulibaly, PM., Henriques, J., Bardiès, M., Darcourt, J., Gardin, I., Buvat, I. . Quantification in SPECT : myth or reality ? A multicentric study. . *IEEE Nuclear Science Symposium Conference Record.* 2004; 5: 3170-3317.
14. Graham LS, Fahey FH, Madsen MT, van Aswegen A, Yester MV. Quantitation of SPECT performance: Report of Task Group 4, Nuclear Medicine Committee. *Med Phys.* 1995; 22: 401-409.
15. Hendel RC, Corbett JR, Cullom SJ, DePuey EG, Garcia EV, Bateman TM. The value and practice of attenuation correction for myocardial perfusion SPECT imaging: a joint position statement from the American Society of Nuclear Cardiology and the Society of Nuclear Medicine. *J Nucl Cardiol.* 2002; 9: 135-143.
16. Zaidi H, Koral KF. Scatter modelling and compensation in emission tomography. *Eur J Nucl Med Mol Imaging.* 2004; 31: 761-782.

17. Hudson HM, Larkin RS. Accelerated image reconstruction using ordered subsets of projection data. *IEEE Trans Med Imaging* 1994; 13: 601-609.

18. Meikle SR, Hutton BF, Bailey DL. A transmission-dependent method for scatter correction in SPECT. *J Nucl Med* 1994; 35: 360-367.

19. Iida H, Narita Y, Kado H, et al. Effects of scatter and attenuation correction on quantitative assessment of regional cerebral blood flow with SPECT. *J Nucl Med.* 1998; 39: 181-189.

20. Narita Y, Eberl S, Iida H, et al. Monte Carlo and experimental evaluation of accuracy and noise properties of two scatter correction methods for SPECT. *Phys Med Biol* 1996; 41: 2481-2496.

21. Narita Y, Iida H, Eberl S, Nakamura T. Monte Carlo evaluation of accuracy and noise properties of two scatter correction methods for ^{201}Tl cardiac SPECT. *IEEE Trans Nucl Sci.* 1997; 44: 2465-2472.

22. Willowson K, Bailey DL, Baldock C. Quantitative SPECT reconstruction using CT-derived corrections. *Phys Med Biol.* 2008; 53: 3099-3112.

23. Kim K, Watabe H, Hayashi T, et al. Quantitative Mapping of Basal and Vasareactive Cerebral Blood Flow using Split-Dose ^{123}I-Idoamphetamine and Single Photon Emission Computed Tomography. *Neuroimage.* 2006; in press.

24. Kim KM, Watabe H, Shidahara M, Ishida Y, Iida H. SPECT collimator dependency of scatter and validation of transmission dependent scatter compensation methodologies. *IEEE Trans Nucl Sci* 2001; 48: 689-696.

25. Kim KM, Watabe H, Hayashi T, et al. Quantitative mapping of basal and vasareactive cerebral blood flow using split-dose (123)I-iodoamphetamine and single photon emission computed tomography. *Neuroimage.* 2006.

26. Iida H, Itoh, H., Nakazawa, M., Hatazawa, J., Nishimura, H., Onishi, Y., Uemura, K., . Quantitative mapping of regional cerebral blood flow using iodine-123-IMP and SPECT. *J Nucl Med* 1994; 35: 2019-2030.

27. Shidahara M, Watabe H, Kim KM, et al. Evaluation of a commercial PET tomograph-based system for the quantitative assessment of rCBF, rOEF and $rCMRO_2$ by using sequential administration of ^{15}O-labeled compounds. *Ann Nucl Med.* 2002; 16: 317-327.

28. Iida H, Higano S, Tomura N, et al. Evaluation of regional differences of tracer appearance time in cerebral tissues using [^{15}O] water and dynamic positron emission tomography. *J Cereb Blood Flow Metab* 1988; 8: 285-288.

29. Iida H, Kanno I, Miura S, Murakami M, Takahashi K, Uemura K. Error analysis of a quantitative cerebral blood flow measurement using $H_2{}^{15}O$ autoradiography and positron emission tomography, with respect to the dispersion of the input function. *J Cereb Blood Flow Metab.* 1986; 6: 536-545.

30. Iida H, Kanno I, Miura S, Murakami M, Takahashi K, Uemura K. A determination of the regional brain/blood partition coefficient of water using dynamic positron emission tomography. *J Cereb Blood Flow Metab* 1989; 9: 874-885.

31. Iida H, Shoji Y, Sugawara S, et al. Design and Experimental validation of a Quantitative myocardial ^{201}Tl SPECT System. *IEEE Trans Nucl Sci.* . 1999; 46: 720-726.

32. Narita Y, Iida H. [Scatter correction in myocardial thallium SPECT: needs for optimization of energy window settings in the energy window-based scatter correction techniques]. *Kaku Igaku.* 1999; 36: 83-90.

33. Iida H, Itoh H, Bloomfield PM, et al. A method to quantitate cerebral blood flow using a rotating gamma camera and iodine-123 iodoamphetamine with one blood sampling. *Eur J Nucl Med Mol Imaging.* 1994; 21: 1072-1084.

34. Iida H, Nakazawa M, Uemura K. [Quantitation of regional cerebral blood flow using 123I-IMP from a single SPECT scan and a single blood sampling--analysis on statistical error source and optimal scan time]. *Kaku Igaku.* 1995; 32: 263-270.

35. Eberl S, Kanno I, Fulton RR, Ryan A, Hutton BF, Fulham MJ. Automated interstudy image registration technique for SPECT and PET. *J Nucl Med.* 1996; 37: 137-145.

36. Kurisu R, Ogura T, Takikawa S, Saito H, Nakazawa M, Iida H. [Estimation and optimization of the use of standard arterial input function for split-dose administration of N-isopropyl-p[^{123}I]iodoamphetamine]. *Kaku Igaku.* 2002; 39: 13-20.

37. Ogura T, Takikawa S, Saito H, Nakazawa M, Shidahara M, Iida H. [Validation and optimization of the use of standardized arterial input function in N-isopropyl-p[123I]iodoamphetamine cerebral blood flow SPECT]. *Kaku Igaku.* 1999; 36: 879-890.

Figure Legend

Table 1: List of gamma camera models and collimators, well counters used by the participating institutions. The Becquerel and cross calibration factors are also listed. The %-True Activity Conc. is ratio of the phantom activity estimated with SPECT and BCF to the known amount of activity in the phantom expressed as a percentage (mean +/- 1 standard deviation: 87.5 +/- 5.1%).

Collimator abbreviations: LMEHRfan – low to medium energy high resolution fan beam, SMS-fan –Siemens Medical Systems fan beam, LEHR – low energy high resolution parallel hole, LEGP.PAR – low energy, general purpose parallel hole, LMEGP – low to medium energy general purpose parallel hole.

Figure 1: Diagram depicting the scanning protocol flow for the DTARG procedure. ^{123}I-IMP for the resting part is injected at time t=0 min and the 28 min initial dynamic SPECT scan is commenced. A blood sample for the calibration of the population input function is drawn at t=10 min and acetazolamide (DMX – diamox) is administered at t=20 min. The last frame (t=24 to 28 min) is used for scaling the CBF values. The second injection of ^{123}I-IMP is performed at t=30 min and the second dynamic SPECT scan is also commenced.

Figure 2: Diagram illustrating the quantitative reconstruction protocol. The emission data are initially reconstructed with filtered back projection (top right image) to allow the brain outline to be determined and μ-map for attenuation correction to be determined by assigning a uniform attenuation coefficient of 0.166 cm^{-1} to the detected brain volume. The μ-map is forward projected to provide the attenuation projections for the scatter correction (bottom right image) as well as used by the OSEM reconstruction for attenuation correction. Scatter correction is carried out on the acquired emission projections using TDCS and the generated attenuation projections.

Figure 3: Line sources images (top row) and profiles through line sources images (bottom row) before and after TDCS scatter correction for two different collimators. Arrows in the lower column indicate the range of the cylinder phantom. The higher energy LMEGP (low to medium energy) collimator of the Toshiba-ECAM camera exhibits less scatter and septal penetration compared to the low energy collimator (LEHR) of the GE system. This also translates into improved scatter and septal penetration removal for the LMEGP collimator. A lower estimated offset component for septal penetration ("DC" component) for the LMEGP (DC=0.05) supports the observation of lower septal penetration compared to the LEHR collimator (DC=0.20).

Figure 4: Reconstructed slices through the uniform phantom from each of the 12 institutions taking part in the evaluation. The phantom experiment was designed to have the same activity concentration in the phantom for each centre's study. Non-uniformities and also differences in absolute activity concentration estimates can be observed, highlighting the need for rigorous calibration, flood correction and QC. Legend above each image gives institution number (same as in Table 1), gamma camera model and collimator used. Collimator abbreviations are as described in legend of Table 1.

Figure 5a: Images from the reproducibility study. CBF images obtained at rest (top row) and after acetazolamide (2nd row) with the DTARG, single session spilt dose procedure. Repeat scan (3rd row) within one month using IMPARG methods and acetazolamide stress (columns 1-3) and at rest (the last column). The images demonstrate that the cerebral vascular reactivity can be estimated with this absolute quantitation technique and demonstrate good reproducibility of measuring both rest and post acetazolamide challenge CBF.

Figure 5b: Typical example of CBF images from the reproducibility study obtained from a single subject at Institution #1. CBF images obtained at rest (top row) and after acetazolamide (2nd row) with the DTARG, single session spilt dose procedure. Repeat

scan (3rd row) within one month using IMPARG method and acetazolamide stress.

Figure 5c: Bland-Altman plot showing the difference between the CBF values estimated from the DTARG and repeat IMPARG studies versus CBF estimated from the IMPARG studies performed to assess reproducibility. Little systematic bias is detected between the two methods (mean difference -0.4 ml/100g/min) and standard deviation of the differences is moderate (5.2 ml/100g/min). The correlation coefficient of $r=0.93$ ($p<0.001$) was found in the linear-regression analysis.

Figure 6a: Comparison of the DTARG measured CBF at rest and after acetazolamide stress with corresponding measurements with ^{15}O-water PET ("VS PET" evaluation) in a patient with left internal-carotid artery stenosis. Rest CBF does not show abnormality but acetazolamide CBF shows defect in the left MCA region. Post reconstruction Gaussian filter was not applied to SPECT CBF in this display.

Figure 6b: Comparison of the DTARG measured CBF at rest and after acetazolamide stress with corresponding measurements with ^{15}O-water PET ("vs PET" evaluation) in a patient with right internal-carotid artery stenosis and left internal-carotid occlusion.. Rest CBF shows defect in the frontal-to-parietal regions, and acetazolamide does not increase CBF in these regions. Post reconstruction Gaussian filter was not applied to SPECT CBF in this display.

Figure 6c: Bland-Altman plot. Moderate underestimation of CBF determined by DTARG compare to PET flow measurements is observed (mean difference of -6.1 ml/100g/min). A correlation coefficient of $r=0.88$ ($p<0.001$) was found in the linear-regression analysis.

Figure 7: Results from the "rest-rest" evaluation carried at two institutions (#2 and #12). In this study the DTARG was performed as per normal protocol except that acetazolamide was not injected. The CBF estimated with the first injection (points on the left of graph) are in good agreement with those estimated with the second injection in the same imaging session (points on the right of the graph).

Table 1. Equipment and Calibration Factor Details

Institution No.	Manifacturer and camera	Number of Detectors	Collimator	BCF	%-True Activity Conc.	Well counter	CCF
1	Toshiba GCA9300	3	N2(LMEHRfan)	72,042	85.3	Counter/Timer SCA-01 (Universal, Tokyo, NaI)	0.972
2	Toshiba GCA9300	3	N2(LMEHRfan)	75,642	87.8	Counter/Timer SCA-01 (Universal, Tokyo, NaI)	0.883
3	Toshiba GCA9300	3	N2(LMEHRfan)	76,348	87.3	Counter/Timer SCA-01 (Universal, Tokyo, NaI)	0.829
4	Siemens ECAM	2	SMS-fan	147,450	99.7	BeWell QS (MIL, Osaka, NaI)	0.769
5	Toshiba ECAM	2	N2(LMEHRfan)	96,173	85.5	Captus300 (Gaointeo, USA, NaI)	0.543
6	GE Millennium VG	2	LEHR	238,601	87.0	Superscaller (Aloka, Tokyo, NaI)	0.845
7	Toshiba ECAM	2	SMS.fan	66,782	78.4	DCM-200 (Aloka, Tokyo, Plastic)	0.160
8	Toshiba ECAM	2	N2(LMEHRfan)	66,627	89.4	DCM-200 (Aloka, Tokyo, Plastic)	0.132
9	Shimadzu IRIX	3	LEGP.PAR	64,902	83.1	Universal TDC-521(Aloka, Tokyo, NaI)	0.834
10	Shimadzu IRIX	3	LEGP.PAR	64,150	91.2	DCM-200 (Aloka, Tokyo, Plastic)	0.134
11	Toshiba ECAM	2	LMEGP.PAR	907,433	89.5	Counter/Timer SCA-01 (Universal, Tokyo, NaI)	0.866
12	Toshiba ECAM	2	LMEGP.PAR	87,175	86.0	Counter/Timer SCA-01 (Universal, Tokyo, NaI)	0.869

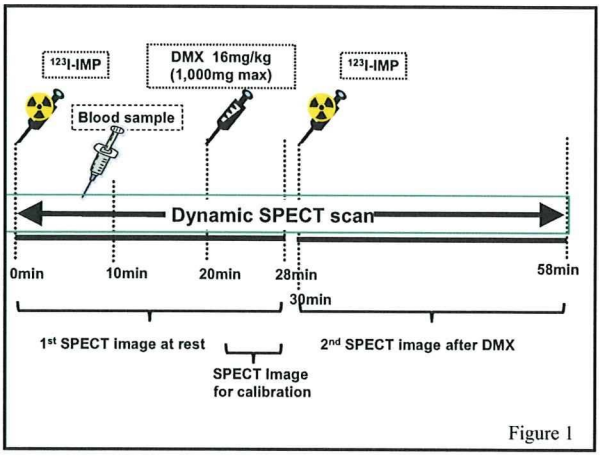

Figure 1

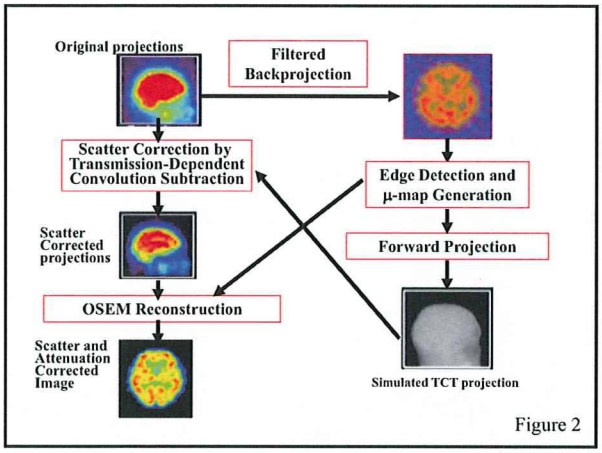

Figure 2

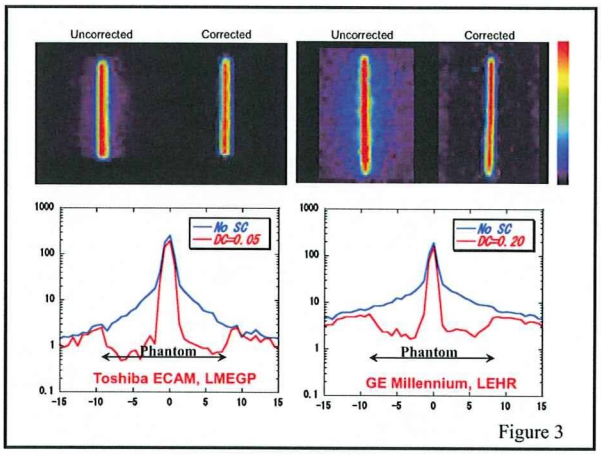

Figure 3

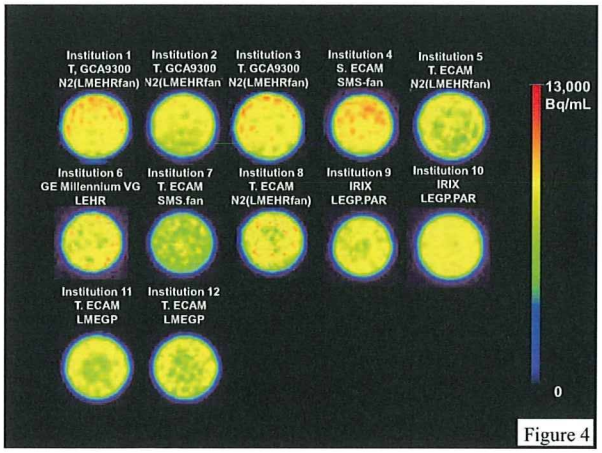

Figure 4

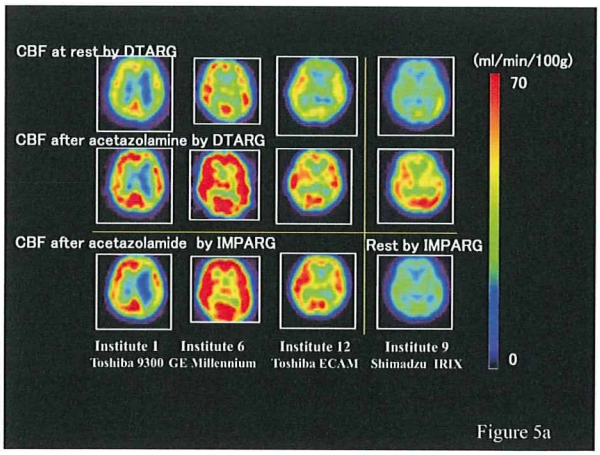

Figure 5a

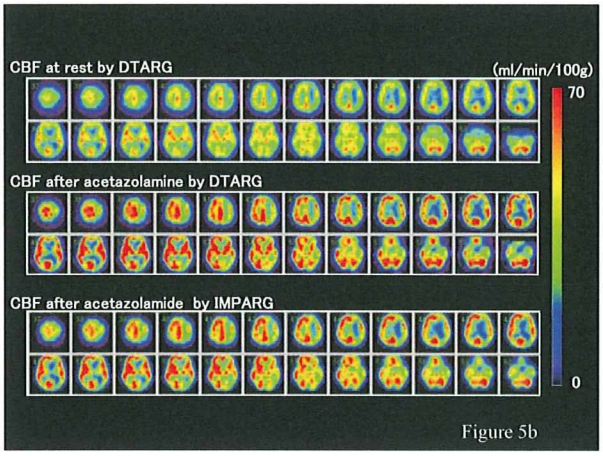

Figure 5b

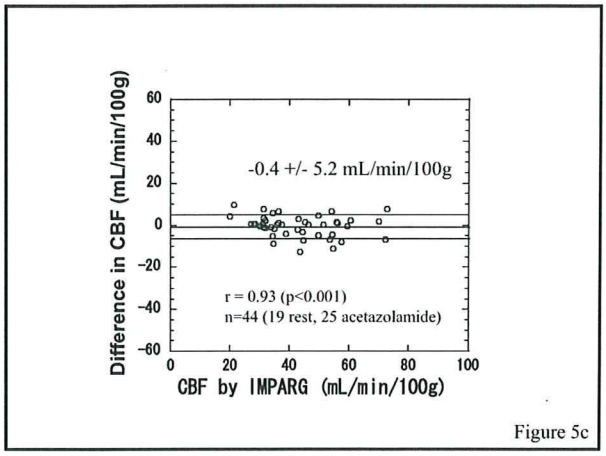

Figure 5c

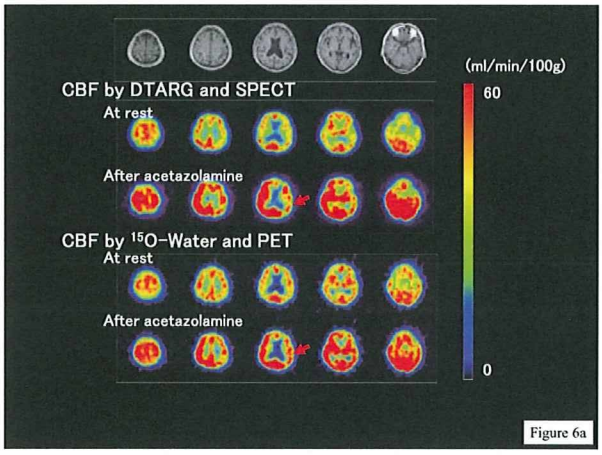

Figure 6a

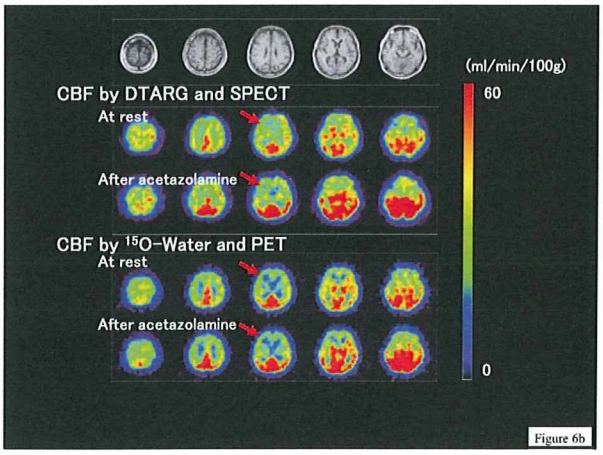

Figure 6b

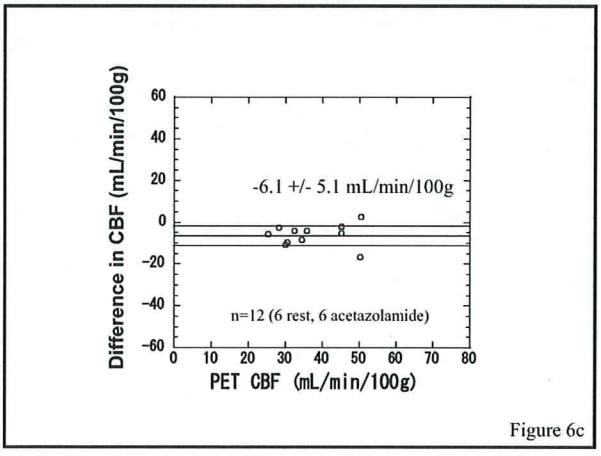

Figure 6c

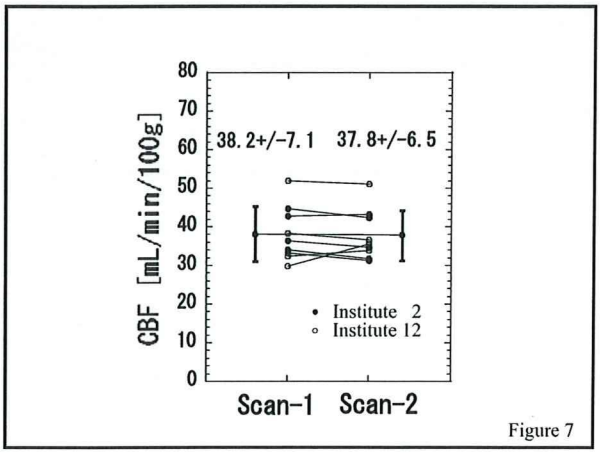

Figure 7